Dalton Transactions

Accepted Manuscript

This is an *Accepted Manuscript*, which has been through the Royal Society of Chemistry peer review process and has been accepted for publication.

Accepted Manuscripts are published online shortly after acceptance, before technical editing, formatting and proof reading. Using this free service, authors can make their results available to the community, in citable form, before we publish the edited article. We will replace this *Accepted Manuscript* with the edited and formatted *Advance Article* as soon as it is available.

You can find more information about *Accepted Manuscripts* in the Information for Authors.

Please note that technical editing may introduce minor changes to the text and/or graphics, which may alter content. The journal's standard Terms & Conditions and the Ethical guidelines still apply. In no event shall the Royal Society of Chemistry be held responsible for any errors or omissions in this *Accepted Manuscript* or any consequences arising from the use of any information it contains.

ROYAL SOCIETY OF CHEMISTRY

www.rsc.org/dalton

Graphical abstract

Palygorskite supported Y_2O_3:(Eu^{3+},Au^{3+}) nanocomposites show simultaneous fluorescence and catalytic activities

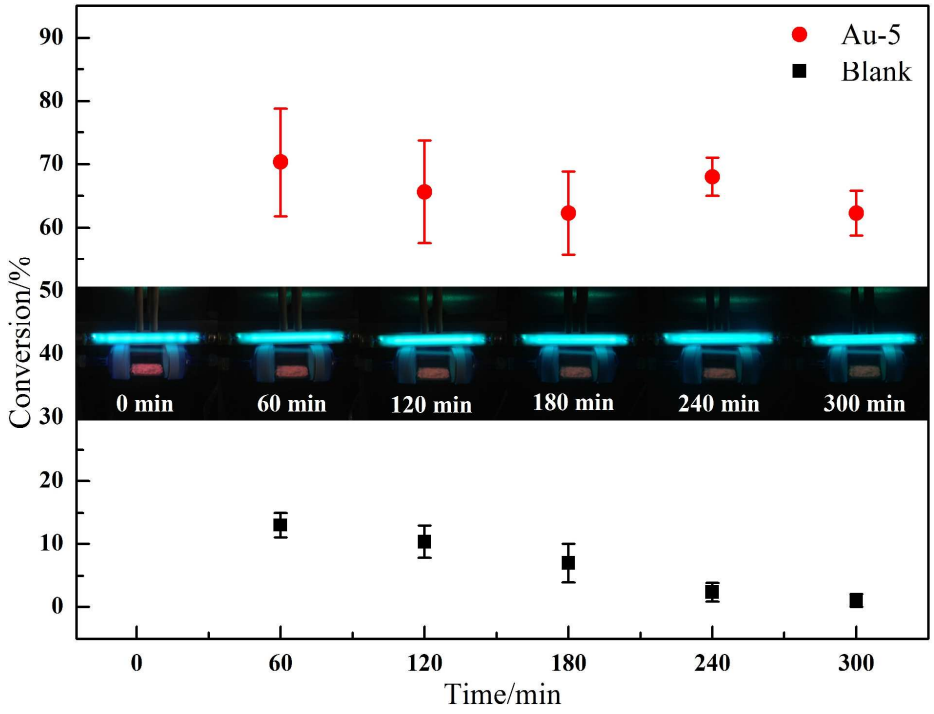

Dalton Transactions Accepted Manuscript

Journal Name

RSCPublishing

PAPER

Fluorescence and room temperature activity of Y_2O_3:(Eu^{3+},Au^{3+})/palygorskite nanocomposite†

Cite this: DOI: 10.1039/x0xx00000x

Xi He and Huaming Yang*

Received 00th January 2014,
Accepted 00th January 2014

DOI: 10.1039/x0xx00000x

www.rsc.org/

The fluorescence and room temperature activity of palygorskite supported Y_2O_3:(Eu^{3+},Au^{3+}) nanocomposite were investigated to design a fluorescence indicated catalyst. The effects of Au^{3+} doping on the structure and surface properties of host material were systematically characterized. The fluorescence intensity of Y_2O_3:Eu^{3+} was affected by Au^{3+} doping, which was related to the crystallinity of Y_2O_3. Excessive Au^{3+} were segregated to the host surface and reduced to metallic Au. The local symmetry of Eu^{3+} was reduced by Au^{3+} doping, which benefited the energy transfer between Eu^{3+} and Au^{3+}. Energy absorbed by Eu^{3+} was transferred from Au^{3+} to metallic Au where electrons were produced. These electrons were absorbed by O_2 to change into O_2^-, which were the oxidant of *ortho*-dichlorobenzene (*o*-DCB). The variation of fluorescence intensity upon catalytic reaction was observed. The room temperature catalytic activity of the nanocomposite under UV irradiation was revealed. The as-synthesized nanocomposite might have a potential application in the environmental fields.

1. Introduction

What if the fluorescence of a composite varies as catalytic reaction goes on? This composite might have interesting applications. For example, it can be an environmental indicator when exposed to harmful pollutants. Its color or fluorescence intensity changes as a result of triggering catalytic reaction. It also can be "nightlights" for cities or highways providing guidance for drivers and purifying vehicle exhaust gas simultaneously.

Gold has been regarded as a novel catalyst in the last decades since the chemical properties of gold nanoparticles and salts in small amounts can differ from those of bulk gold.[1] Quantum size effect in the electronic structure caused by electron confinement to a restricted volume appears to be responsible for the unexpected catalytic properties of Au,[2] which has been applied in many fields.[3-10] Meanwhile, nanosized gold is also used to optimize the fluorescence/optical property through surface plasmon resonances.[11-15] There seems to be some kind of connection hide in catalysis and fluorescence, particularly in the gold-containing system. However, to the best of our knowledge, the connection has never been revealed before, let alone the variation of fluorescence upon catalytic reaction.

Department of Inorganic Materials, School of Minerals Processing and Bioengineering, Central South University, Changsha 410083, China

**Corresponding author, email: hmyang@csu.edu.cn, Tel.: +86-731-88830549, Fax: +86-731-88710804.*

† Electronic supplementary information (ESI) available: DOI: 10.1039/x0xx00000x

Gold catalysis is energy-consuming because heating is favorable to obtain a good activity.[16-20] The connection between fluorescence and catalysis can be established if energy transfer between them is realized. Energy transfer is affected by the interaction between the donor and the acceptor sites/species.[21] Therefore, energy transfer can be affected by doping since it varies the interaction in particles or ions.

Y_2O_3 is a well-accepted fluorescence substrate. It possesses a cubic bixbyite structure (space group *Ia*3) and two distinct crystallographic sites available for rare earth ion substitution.[22,23] Take Y_2O_3:Eu^{3+} for example. The intensity ratio of $^5D_0$-$^7F_2$ to $^5D_0$-$^7F_1$ is closely related to the local environment of Eu^{3+}, which can be used as an indicator to reflect the change of local environment. The larger the intensity ratio, the lower the local symmetry.[24,25] Lowering local symmetry benefits energy transfer.[26-28] Therefore, energy transfer between Eu^{3+} and dopant might be realized if the local symmetry of Eu^{3+} is reduced. Meanwhile, this reducing can be easily reflected by the intensity ratio of $^5D_0$-$^7F_2$ to $^5D_0$-$^7F_1$. Au^{3+} appears to be a proper candidate as its radii is similar to Y^{3+} but smaller than Eu^{3+}, and the low temperature activity of gold nanocomposite for organic pollutant has been suggested in our previous work.[29]

Y_2O_3:(Eu^{3+},Au^{3+})/palygorskite, a fluorescence indicated gold nanocomposite, was reported herein. The connection between fluorescence and room temperature activity was fully investigated. The structure, surface, morphology, fluorescence and catalysis of the nanocomposite were characterized. All the evidence showed that Au^{3+} was successfully doped into Y_2O_3. Metallic Au was only formed on the surface of Au-5. Energy absorbed by Eu^{3+} was

Dalton Transactions Accepted Manuscript

transferred from Au^{3+} to surface metallic Au where O_2^- was produced. The room temperature activity and the variation of fluorescence intensity upon catalytic reaction suggested that energy absorbed in fluorescence could be used in catalysis. The connection between fluorescence and catalysis might spark a novel way for the development of novel catalysts and catalytic equipment.

2. Experimental

2.1 Materials

Palygorskite (Pal) was purchased from Xuyi, China. Ethanol (AR), $HAuCl_4 \cdot 4H_2O$ (AR) and Na_2CO_3 (AR) were purchased from Sinopharm Chemical Reagent Co., Ltd. $Y(NO_3)_3 \cdot 6H_2O$ (4N) was purchased from Sinopharm Chemical Reagent Co., Ltd. $Eu(NO_3)_3 \cdot 6H_2O$ (4N) was purchased from Xiya Reagent. Oleic acid (AR) was purchased from Kermel Reagent.

2.2 Synthesis of Y_2O_3:(Eu^{3+},Au^{3+})/Pal

Pal was dispersed in an ethanol-oleic acid solution and stirred at 60°C for 4 h. The volume ratio of ethanol to oleic acid was 40:1. The mixture was treated with sonication for 15 min before it was mixed with the ions solution. $Y(NO_3)_3 \cdot 6H_2O$, $Eu(NO_3)_3 \cdot 6H_2O$ and $HAuCl_4 \cdot 4H_2O$ were dissolved in deionized water with magnetic stirring (Fig. 1). Oleic acid was added to produce a water-oil system. After being stirred at 25°C for 2 h, pretreated Pal mixture was added and further stirred for 8 h. Alkali (Na_2CO_3, 0.2 mol/L) was dropped at a rate of 100 ml/h to produce Y_2O_3:(Eu^{3+},Au^{3+})/Pal precursor. The precursor was washed twice before drying and calcination. The molar ratio of Y^{3+} to Eu^{3+} was 20:1, while the dosage of Au^{3+} varied with Au-*x*. *X* means the dosage of $HAuCl_4 \cdot 4H_2O$, whose concentration was 0.5 g/L (1.2×10^{-3} mol/L). *X*=1 means 1 ml $HAuCl_4 \cdot 4H_2O$ was added.

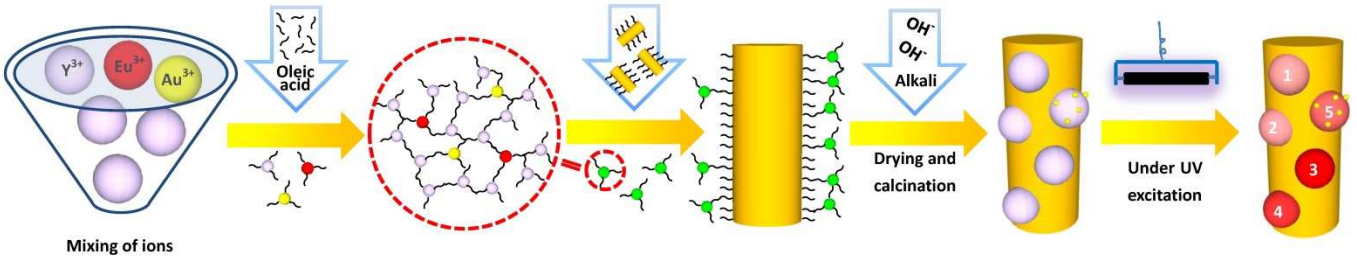

Fig. 1 Illustration for the synthesis of Y_2O_3:(Eu^{3+},Au^{3+})/Pal. Samples with different Au^{3+} content show different fluorescence intensities. Numbers marked in red spheres means the dosage of $HAuCl_4 \cdot 4H_2O$. The PL intensity of Au^{3+} doped Y_2O_3:Eu^{3+} is in the order of Au-1=Au-2<Au-5<Au-4<Au-3, which was also reflected by the color of spheres (the deeper the red, the stronger the intensity).

2.3 Materials characterization

X-ray diffraction (XRD) patterns were recorded using a DX-2700 diffractometer with Cu Kα radiation. Fourier transform infrared (FTIR) spectra were recorded on a Shimadzu FTIR 8120 spectrometer using the dried KBr disk technique, over the range 4000~400 cm^{-1}. X-ray photoelectron spectroscopy (XPS) measurements were performed on a Thermo Fisher Scientific K-Alpha 1063 equipped with a hemispherical electron analyzer and an Al Kα X-ray radiation source. The pressure in the analysis chamber was below 10^{-9} Torr during the analysis. The XPS binding energy (BE) was internally referenced to the C 1s peak (BE=284.8 eV). The scan parameters for Au 4f were 0.05 eV and 25 eV pass energy, while those for the other elements were 0.4 eV and 50 eV pass energy. The sample suspension pretreated with sonication for 15 min was dropped on a copper alloy stub for morphological analysis and composition characterization by a JSM-6360 LV scanning electron microscopy (SEM) equipped with an Oxford EDAX X-ray fluorescent energy-dispersion spectrum (EDS) analyzer. Transmission electron microscopy (TEM) and high resolution transmission electron microscopy (HRTEM) were conducted using a JEM 2100F microscope operated at 200 KeV. The fluorescence spectra were recorded on an F-4500 Fluorescence Spectrophotometer using a 450 W Xe lamp as the excitation source. The PL spectra of all the samples were obtained from the same way. Sample (2.0 g) was pressed (2×10^5 N) into disk with diameter of 10 mm. All these disks (one sample, three disks) were characterized with the same parameters. Finally, the mean values were used for comparison. UV-Vis spectra were recorded on a UV-2450 UV-Vis spectrophotometer equipped with 10 mm quartz cell.

The content of Au^{3+} was very low and the effects of Au^{3+} doping might be interfaced by palygorskite, therefore samples were studied without palygorskite (except in SEM and TEM characterization) to better understand how the properties of Y_2O_3:Eu^{3+} were affected by Au^{3+} doping.

2.4 Catalytic activity measurement

Room temperature catalytic reaction was conducted in a self-design reactor showed in Fig. S1. The feeding flow rate to the reactor was set at 70 ml/min, and *o*-DCB concentration was maintained at 600 ppm by a mass flow controller. 50 mg powders were dispersed on a glass carrier (the area loaded with samples was 5 cm × 2.5 cm), which was fixed in the center of quartz reactor. These glass carriers (loaded with samples) were dried at 60°C for 12 h before catalytic test. All the work reported in this paper was done with a low-pressure mercury lamp, which was rated at 6 W power consumption with 2 W of UV output at 254 nm. The inlet and outlet gases were analyzed by an on-line GC-4000A equipped with a flame ionization detector (FID).

3. Results and discussion

3.1 Effect of Au^{3+} doping on Y_2O_3:Eu^{3+}

Dalton Transactions Accepted Manuscript

This journal is © The Royal Society of Chemistry 2013

Successful doping of Au^{3+} into Y_2O_3 was suggested in XRD (Fig. 2a). All the patterns were Y_2O_3 (PDF#41-1105). Differences among patterns were not obvious as the content of gold was so limited. However, results calculated from XRD showed that the distances of planes decreased as gold dosage increased (Table S1). The radii of Y^{3+}, Eu^{3+} and Au^{3+} were 0.89, 0.96 and 0.85 Å respectively.[30] Therefore, the decreasing in interplanar distances suggested that Au^{3+} had incorporated in the crystal lattice of Y_2O_3. The FWHM of Y_2O_3 decreased from Au-1 to Au-3 but increased from Au-3 to Au-5 (Table S2). Doping with big radii ions led to the deformation of host crystal structure.[31] However, this deformation might be reduced when ions with smaller radii were doped at the same time. This reducing would come to a limited extent when Au^{3+}/Eu^{3+} reached a proper ratio. Therefore, further doping with Au^{3+} ions would break the balance between Eu^{3+} and Au^{3+}. The crystallite size and strain of Au doped samples were listed in Table S3, it is obvious that the effect of strain on the peak shape can be ignored. The structure change of Pal was shown in Fig. S2.

FTIR spectra showed that the surface of Y_2O_3 was partly modified in Au-5 (Fig. 2c). Band at 563 cm^{-1} was the characteristic vibration of Y-O.[32,33] Bands at 869 and 1068 cm^{-1} were the deformation and symmetric stretching model of CO, which were also observed in hydroxyl-carbonate Y_2O_3 precursor.[34] Band at 1486 cm^{-1} suggested the existence of CO_3^{2-}.[32,33,35] Band at 1394 cm^{-1} belonged to the stretching vibration of CO_3^- in $Y(OH)CO_3$,[34,36] which was caused by adsorption of H_2O and CO_2 from air atmosphere. The big band ranged from 2800 to 3700 cm^{-1} was the stretching vibration of physically adsorbed H_2O.[37] The FTIR spectra from Au-1 to Au-4 were almost the same. However, the stretching vibration of physically adsorbed H_2O in Au-5 was greatly reduced. Y_2O_3 reacted with H_2O at room temperature in the following hydrolysis process: Y_2O_3 + physisorbed water → $Y_2O_3{\cdot}H_2O$ (strongly adsorbed on the surface layer) → Y_2O_3 (H_2O bulk species) or YOOH → $Y(OH)_3$.[38] YOOH or $Y(OH)_3$ could further react with CO_2 from air to form hydroxyl-carbonate species. Weakening bands of 869, 1068, 1486, 1394 cm^{-1} and adsorbed H_2O indicated that the surface of Au-5 was inert to H_2O or CO_2. Excessive Au^{3+} in Au-5 might be segregated to the surface in the form of Au_2O_3. Therefore, metallic Au was formed on the surface of Y_2O_3 because Au_2O_3 was easily decomposed to metallic Au[39,40] and high temperature was necessary in producing Y_2O_3:Eu^{3+} (Fig. S3).

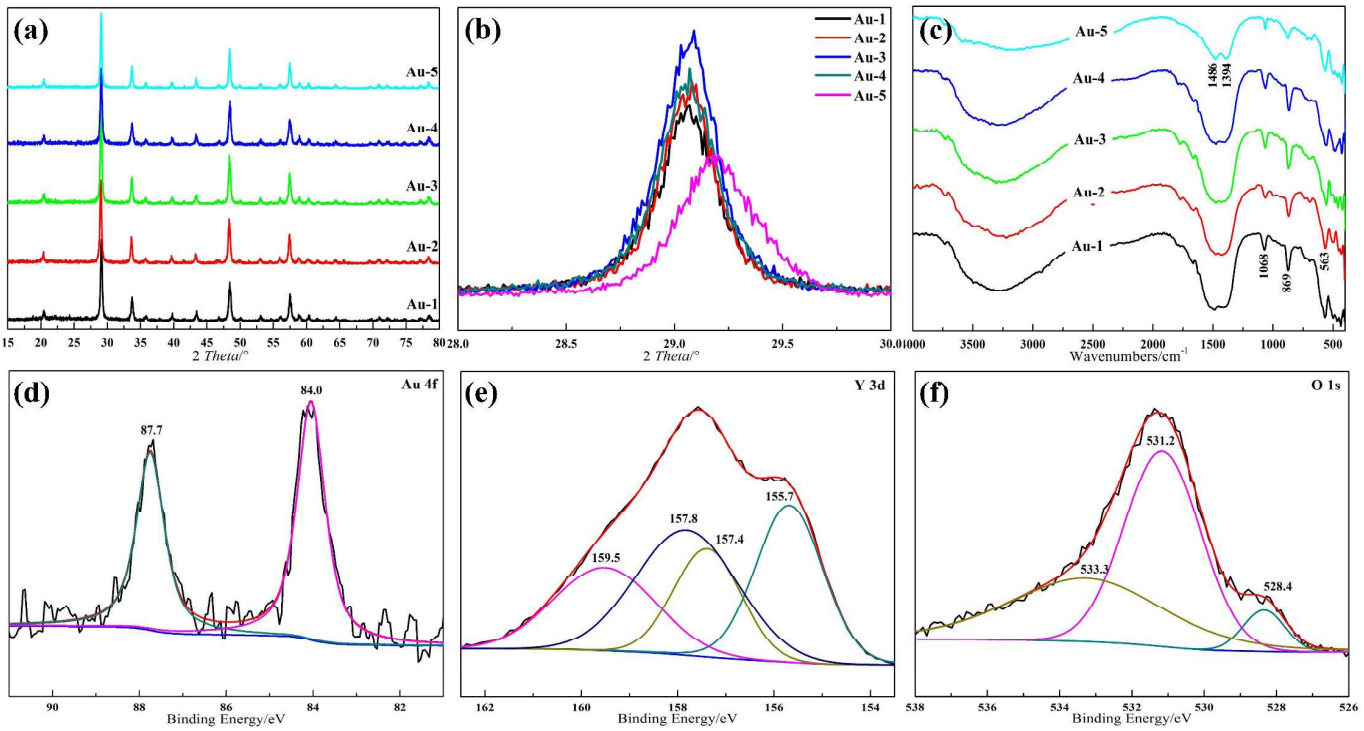

Fig. 2 (a,b) XRD patterns, (c) FTIR spectra of Au^{3+} doped samples, and XPS spectra of (d) Au 4f, (e) Y 3d, (f) O 1s in Au-5. The intensities in (a, b,c) were normalized.

3.2 Existence form of Au species

XPS was employed to certify Au species in Au-5 (Fig. 2d). The binding energies at 84.0 and 87.7 eV corresponded to metallic Au with Au $4f_{7/2}$ and Au $4f_{5/2}$ in the Au 4f spectra (Fig. 2d), respectively, which coincided with the results reported previously.[39-42] However, the binding energies demonstrating the existence of Au^{3+} were not observed in Au-5 and the other four Au doped samples (Fig. S4),[43-45] indicating that Au^{3+} was buried in the interior of the samples. The fitting of O 1s (Fig. 2e) region with three peaks indicated that three kinds of oxygen species existed in the near surface domain of Y_2O_3. The O 1s binding energy at 528.4 eV was lower than that of crystal lattice oxygen.[38,46] The oxygen was associated with reduced yttrium centers (Fig. 2f) because Y^{3+} could get electrons from Au.[47,48] Binding energy at 531.2 eV was attributed to hydroxyl groups on the surface of nanoparticles, and binding energy at 533.3 eV belonged to

Dalton Transactions Accepted Manuscript

oxygen of adsorbed water.[46,49] Binding energy at 155.7 eV was assigned to reduced yttrium, while those at 157.4 and 159.5 eV were attributed to Y_2O_3.[48,50-52] However, lower binding energies of O 1s and Y 3d were not observed in Y_2O_3:Eu^{3+} (Fig. S5).

Fig. 3 shows the morphologies of Au-5. Interplanar distances of 3.04, 3.05 and 3.06 Å belonged to Y_2O_3 (PDF#41-1105), while that of 3.20 and 2.01 Å were from Au_2O_3 (PDF#43-1039) and metallic Au (PDF#04-0784), respectively. More interplanar distances were shown in Fig. S6. Interplanar distances of Y_2O_3 were reduced by Au^{3+} doping as some of these values were smaller than standard values. Obvious contrast between the lattice fringes of metallic Au and Y_2O_3 could be observed if they were not in the same level. However, the lattice fringes of both were apparent. Therefore, metallic Au particles with diameter of 5 nm were coated on Y_2O_3 like a layer. SEM images of Y_2O_3:(Eu^{3+},Au^{3+}) and Y_2O_3:(Eu^{3+},Au^{3+})/Pal were shown in Fig. S7 and Fig. S8. The dispersion of Y_2O_3:(Eu^{3+},Au^{3+}) was improved when Pal was used as the support.

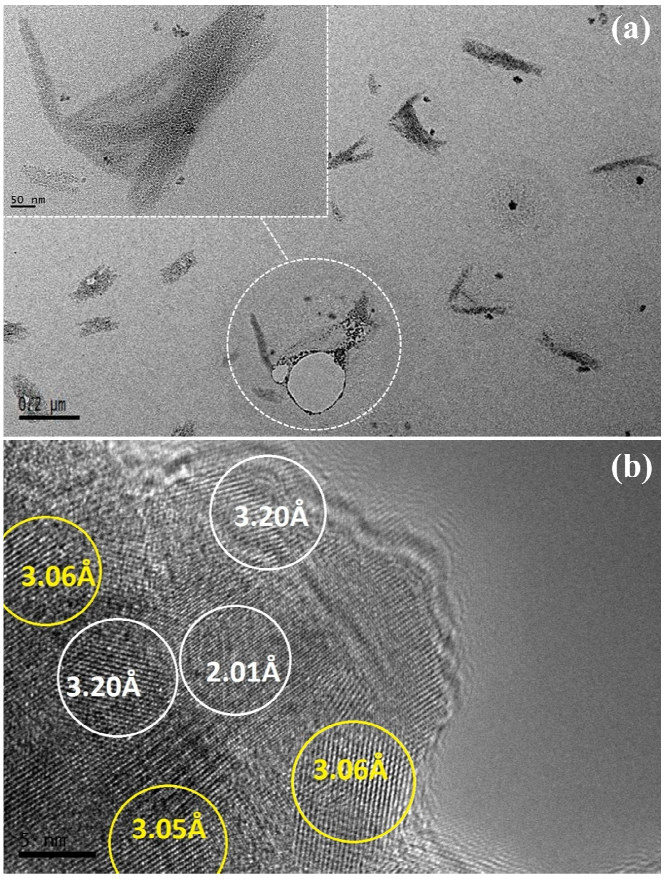

Fig. 3 (a) TEM and (b) HRTEM images of Au-5 sample.

3.3 Effect of Au doping on the local environment of Eu^{3+}

Fluorescence spectra not only showed excitation level of activators but also reflected their local environment. Fig. 4a shows the emission spectra of Y_2O_3:(Eu^{3+},Au^{3+}) excited at 254 nm. The green emission at 535 nm belonged to $^5D_1$-$^7F_1$ (the emission of $^5D_1$-$^7F_1$ is dominant compared with other emissions of $^5D_1$ which are too weak to detect).[53] Emission at 580 nm corresponded to $^5D_0$-$^7F_0$, emissions between 586-600 nm belonged to $^5D_0$-$^7F_1$.[54,55] The strongest emission at 612 nm corresponded to $^5D_0$-$^7F_2$.[24,56,57] Emissions at 650 and 707 nm were from $^5D_0$-$^7F_3$ and $^5D_0$-$^7F_4$, respectively.[54] The intensity of $^5D_0$-$^7F_2$ increased from Au-1 to Au-3 then decreased from Au-3 to Au-5. The enhancement of fluorescence intensity was due to the increasing of crystallinity.[58]

The ratio of $^5D_0$-$^7F_2$ to $^5D_0$-$^7F_1$ was closely related to the local environment of Eu^{3+}.[53] The larger the ratio, the lower the local symmetry.[24,25] The ratio of Y_2O_3:(Eu^{3+},Au^{3+}) was bigger than that of Y_2O_3:Eu^{3+} (Table 1), indicating that the local symmetry was reduced by Au^{3+} doping. The $^5D_0$-$^7F_2$ transition was electric dipole forbidden in crystal sites that have inversion symmetry, which means that Eu^{3+} at C_2 site contributes to $^5D_0$-$^7F_2$ transition. However, Eu^{3+} at C_2 and C_{3i} sites both contribute to the $^5D_0$-$^7F_1$ transition. The ratio of $^5D_0$-$^7F_2$ to $^5D_0$-$^7F_1$ increased from Au-1 to Au-5 (Table 1). High ratio in Au^{3+} doped samples means some of Eu^{3+} in C_{3i} sites were substituted by Au^{3+}. Therefore, substituted Eu^{3+} was pushed to C_2 sites, and more $^5D_0$-$^7F_2$ transition was observed. The local symmetry was reduced as Eu^{3+} was pushed from C_{3i} to C_2 sites, and energy transfer was promoted.

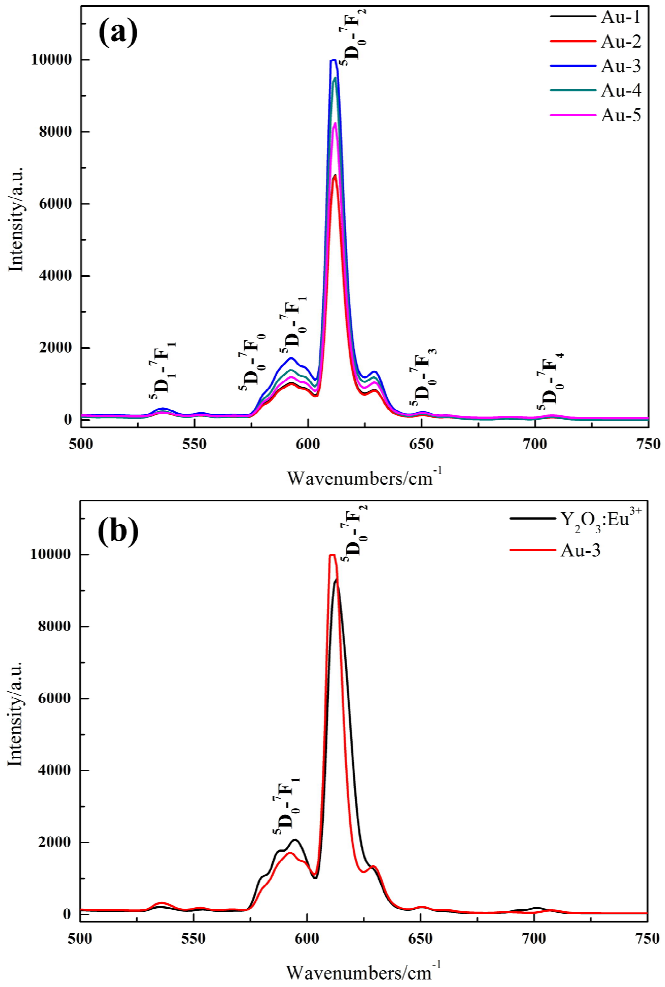

Fig. 4 Room temperature fluorescence of different samples.

Dalton Transactions Accepted Manuscript

This journal is © The Royal Society of Chemistry 2013

Table 1 Ratio of $^5D_0$-$^7F_2$ to $^5D_0$-$^7F_1$ in different samples.

Sample	Y_2O_3:Eu^{3+}	Au-1	Au-2	Au-3	Au-4	Au-5
Ratio	4.47	6.63	6.81	--	6.85	6.95

Note: The ratio of Au-3 is failed to obtain as the $^5D_0$-$^7F_2$ intensity exceeds the detection limit of the equipment, however, the trend caused by Au^{3+} doping is still obvious.

3.4 Room temperature activity of Au-5

The possibility of Au-5 as a catalyst was proposed based on the analysis mentioned above. Interestingly, Au-5 showed good catalytic activity for *o*-DCB at room temperature (Fig. 5). Meanwhile, the fluorescence intensity variation upon catalytic reaction grabbed our greatest attention. To the best of our knowledge, this phenomenon has not been reported before. Energy was transferred from Eu^{3+} to surface metallic Au as surface plasmon resonances of Au was not obvious (Fig. S9) and metal ions/atom pairs could transfer energy.[59] Schematic diagram of Eu^{3+}, Au^{3+} co-doping and energy transfer was depicted in Fig. 6. Energy absorbed by Eu^{3+} under UV irradiation was transferred from Au^{3+} to surface metallic Au where O_2^- were produced, similar to reported results.[60] Therefore, *o*-DCB was completely decomposed under the attack of O_2^-. The formation of O_2^- was also proved in degradation of methylene blue (Fig. S10), and energy transfer in Au-5 was also suggested by the resistance experiment (Fig. S11).

Defects in the host matrix acted as non-radiative recombination centers that reduce the fluorescence intensity.[61] Metallic Au could cut or weaken the Y-O bond to benefit the escape of oxygen, providing opportunities to generate oxygen vacancies and release free electrons.[29] Therefore, the fluorescence intensity decreased as catalytic reaction goes on. However, the fluorescence intensity would partly recover when *o*-DCB was exhausted and completely recover when Au-5 was calcined in sufficient oxygen atmosphere. Moreover, the fluorescence intensity maintained the same when the concentration of *o*-DCB was zero.

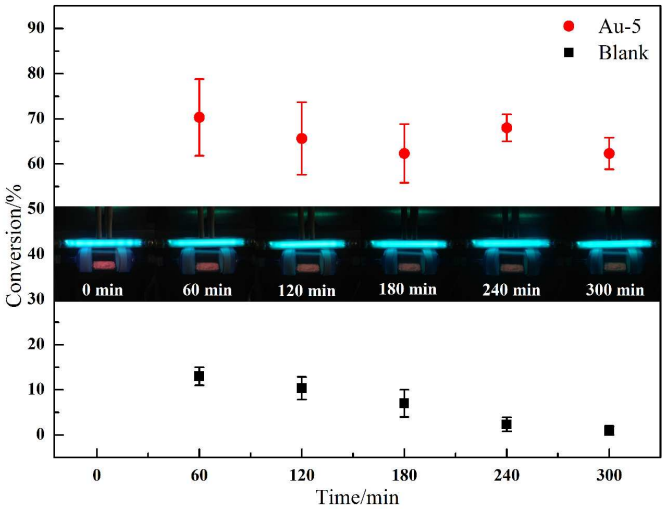

Fig. 5 Catalytic test and fluorescence intensity variation upon catalytic reaction of Au-5. Photographs were taken at every 1 h by a digital camera with focusing on the center of the glass carrier.

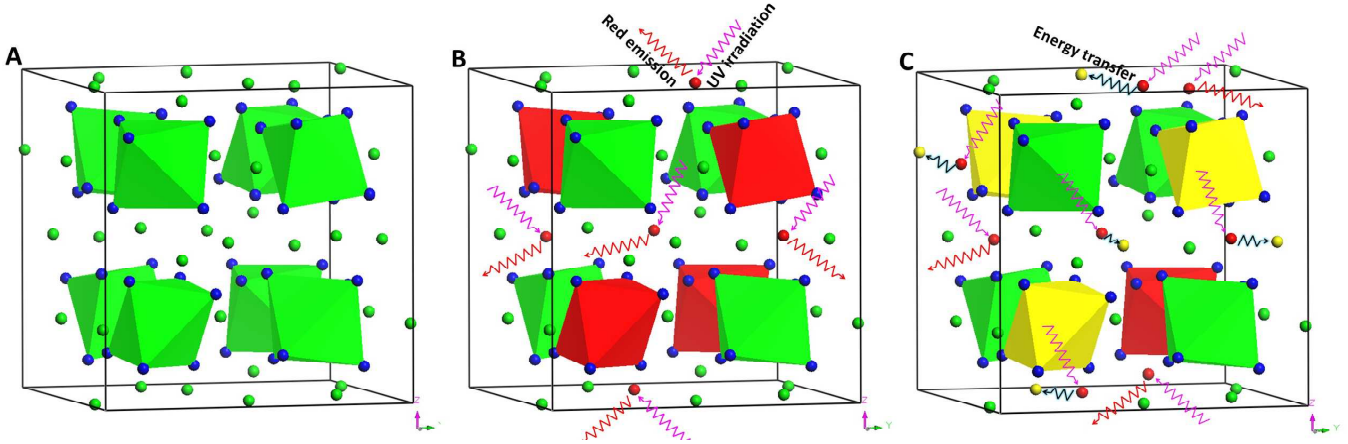

Fig. 6 Schematic diagram of Eu^{3+}, Au^{3+} co-doping and energy transfer. Balls marked in green, red, yellow and blue are Y^{3+}, Eu^{3+}, Au^{3+} and O^{2-} respectively. C_{3i} sites locate inside of octahedral which are surrounded by C_2 sites. The red and yellow octahedral means the C_{3i} sites are occupied by Eu^{3+} and Au^{3+}, respectively. A shows the Y_2O_3 lattice without doping. B is Eu^{3+} doped Y_2O_3, Eu^{3+} would occupy C_2 or C_{3i} sites and give red emission under UV irradiation. However, Eu^{3+} would be pushed from C_{3i} to C_2 sites when Au^{3+} are added, which would reduce the local symmetry of Eu^{3+}. The reducing of local symmetry benefits energy transfer between Eu^{3+} and Au^{3+}. Therefore, the energy absorbed by Eu^{3+} is partially transferred from Au^{3+} to surface metallic Au where the catalytic reaction is triggered.

4. Conclusions

Y_2O_3:(Eu^{3+},Au^{3+})/Pal was successfully synthesized via a co-precipitation method. The fluorescence variation of Y_2O_3:Eu^{3+} and the room temperature activity of Au-5 were caused by Au^{3+} doping. The local symmetry of Eu^{3+} was reduced by Au^{3+} doping, which benefited energy transfer. Absorbed energy was transferred from Eu^{3+} to Au^{3+} and to surface metallic Au where electrons were produced. O_2 absorbed these electrons to change into O_2^-, which were the active species of oxidation. The highlight of this work is

Dalton Transactions Accepted Manuscript

that the hidden connection between fluorescence and catalysis for gold was revealed. Moreover, the fluorescence intensity varies upon catalytic reaction, the as-synthesized nanocomposite might have potential application in the field of environmental catalysis.

Acknowledgements

This work was supported by the National Science Fund for Distinguished Young Scholars (51225403), the Specialized Research Fund for the Doctoral Program of Higher Education (20120162110079), the Hunan Provincial Natural Science Fund for Innovative Research Groups (201302) and Hunan Provincial Innovation Foundation for Postgraduates (CX2012B122).

Notes and references

1 G.J. Hutchings, *Catal. Today*, 2005, **100**, 55-61.
2 H.-G. Boyen, G. Kästle, F. Weigl, B. Koslowski, C. Dietrich, P. Ziemann, J.P. Spatz, S. Riethmüller, C. Hartmann, M. Möller, G. Schmid, M.G. Garnier and P. Oelhafen, *Science*, 2002, **297**, 1533-1536.
3 M. Rodríguez-Castillo, D. Laurencin, F. Tielens, A. van der Lee, S. Clément, Y. Guari and S. Richeter, *Dalton Trans.*, 2014, **43**, 5978-5982.
4 R. Liu, J. Liu, W. Kong, H. Huang, X. Han, X. Zhang, Y. Liu and Z. Kang, *Dalton Trans.*, 2014, DOI: 10.1039/C4DT00630E.
5 D.-M. Tang, L. Chang, J.-W. Yu, L.-L. Zhang, P.-X. Hou, J.-C. Li, F. Li, Y. Bando, D. Golberg and H.-M. Cheng, *ACS Nano,* 2014, **8**, 292-301.
6 S. Li, H. Zhu, Z. Qin, G. Wang, Y. Zhang, Z. Wu, Z. Li, G. Chen, W. Dong, Z. Wu, L. Zheng, J. Zhang, T. Hu and J. Wang, *Appl. Catal. B*, 2014, **144**, 498-506.
7 P.J. Chueh, R.-Y. Liang, Y.-H. Lee, Z.-M. Zeng and S.-M. Chuang, *J. Hazard. Mater.*, 2014, **264**, 303-312.
8 J. Carreras, G. Gopakumar, L. Gu, A. Gimeno, P. Linowski, J. Petuškova, W. Thiel and M. Alcarazo, *J. Am. Chem. Soc.*, 2014, **135**, 18815-18823.
9 F. Menegazzo, M. Signoretto, F. Pinna, M. Manzoli, V. Aina, G. Gerrato and F. Boccuzzi, *J. Catal.*, 2014, **309**, 241-247.
10 S. Xiang, Y. Zhou, Y. Zhang, Z. Zhang, X. Sheng, S. Zhou and Z. Yang, *Dalton Trans.*, DOI: 10.1039/C4DT00882K.
11 C.W. Cheng, E.J. Sie, B. Liu, C.H.A. Huan, T.C. Sum, H.D. Sun and H.J. Fan, *Appl. Phys. Lett.*, 2010, **96**, 071107.
12 J.B. González-Díaz, A. García-Martín, J.M. García-Martín, A. Cebollada, G. Armelles, B. Sepúlveda, Y. Alaverdyan and M. Käll, *Small*, 2008, **4**, 202-205.
13 M.S. Kim, D.H. Park, E.H. Cho, K.H. Kim, Q.-H. Park, H. Song, D.-C. Kim, J. Kim and J. Joo, *ACS Nano*, 2009, **3**, 1329-1334.
14 T. Tozawa, *Chem. Commun.*, 2004, 1904-1905.
15 J. Lee, A.O. Govorov, J. Dulka and N.A. Kotov, *Nano Lett.*, 2004, **4**, 2323-2330.
16 A. Corma and H. Garcia, *Chem. Soc. Rev.*, 2008, **37**, 2096-2126.
17 A. Corma and P. Serna, *Science*, 2006, **313**, 332-334.
18 M.D. Hughes, Y.-J. Xu, P. Jenkins, P. McMorn, P. Landon, D.I. Enache, A.F. Carley, G.A. Attard, G.J. Hutchings, F. King, E.H. Stitt, P. Johnston, K. Griffin and C.J. Kiely, *Nature*, 2005, **437**, 1132-1135.
19 Q. Fu, H. Saltsburg and M. Flytzani-Stephanopoulos, *Science*, 2003, **301**, 935-938.
20 M. Yang, L.F. Allard and M. Flytzani-Stephanopoulos, *J. Am. Chem. Soc.*, 2013, **135**, 3768-3771.
21 J. Bang, H. Yang and P.H. Holloway, *J. Chem. Phys.*, 2005, **123**, 084709.
22 F. Vetrone, J.-C. Boyer, J.A. Capobianco, A. Speghini and M. Bettinelli, *Chem. Mater.*, 2003, **15**, 2737-2743.
23 S. Chandra, F.L. Deepak, J.B. Gruber and D.K. Sardar, *J. Phys. Chem. C*, 2010, **114**, 874-880.
24 A.P. Jadhav, A. Pawar, C.W. Kim, H.G. Cha, U. Pal and Y.S. Kang, *J. Phys. Chem. C*, 2009, **113**, 16652-16657.
25 T. Myint, R. Gunawidjaja and H. Eilers, *J. Phys. Chem. C*, 2012, **116**, 1687-1693.
26 W. Choe, Y.-H. Kiang, Z. Xu and S. Lee, *Chem. Mater.*, 1999, **11**, 1776-1783.
27 Y.V. Suleimanov and A.A. Buchachenko, *J. Phys. Chem. A*, 2007, **111**, 8959-8967.
28 T. Ansbacher, H.K. Srivastava, T. Stein, R. Baer, M. Merkx and A. Shurki, *Phys. Chem. Chem. Phys.*, 2012, **14**, 4109-4117.
29 X. He and H. Yang, *J. Mol. Catal. A*, 2013, **379**, 219-224.
30 R.D. Shannon, *Acta Crystallogr.*, 1976, **A32**, 751-767.
31 B. Cheng, Z. Zhang, H. Liu, Z. Han, Y. Xiao and S. Lei, *J. Mater. Chem.*, 2010, **20**, 7821-7826.
32 L. Muresan, E.-J. Popovici, R. Grecu and L.B. Tudoran, *J. Alloys Compd.*, 2009, **471**, 421-427.
33 M.K. Devaraju, S. Yin and T. Sato, *Inorg. Chem.*, 2011, **50**, 4698-4704.
34 M.I. Martinez-Rubio, T.G. Ireland, G.R. Fern, J. Silver and M.J. Snowden, *Langmuir*, 2001, **17**, 7145-7149.
35 F. Vetrone, J.C. Boyer, J.A. Capobianco, A. Speghini and M. Bettinelli, *J. Phys. Chem. B*, 2003, **107**, 1107-1112.
36 C.A. Traina and J. Schwartz, *Langmuir*, 2007, **23**, 9158-9161.
37 G. Pan, H. Song, X. Bai, L. Fan, H. Yu, Q. Dai, B. Dong, R. Qin, S. Li, S. Lu, X. Ren and H. Zhao, *J. Phys. Chem. C*, 2007, **111**, 12472-12477.
38 Y. Kuroda, H. Hamano, T. Mori, Y. Yoshikawa and M. Nagao, *Langmuir*, 2000, **16**, 6937-6947.
39 H. Tsai, E. Hu, K. Perng, M. Chen, J.-C. Wu and Y.-S. Chang, *Surf. Sci.*,2003, **537**, L447-L450.
40 L.K. Ono and B.R. Cuenya, *J. Phys. Chem. C*, 2008, **112**, 4676-4686.
41 J. Torres, C.C. Perry, S.J. Bransfield and D.H. Fairbrother, *J. Phys. Chem. B*, 2002, **106**, 6265-6272.
42 Yu. Mikhlin, M. Likhatski, Ye. Tomashevich, A. Romanchenko, S. Erenburg and S. Trubina, *J. Electron. Spectrosc. Relat. Phenom.*, 2010, **177**, 24-29.
43 E.D. Park and J.S. Lee, *J. Catal.*, 1999, **186**, 1-11.
44 F.-W. Chang, H.-Y. Yu, L.Selva Roselin, H.-C. Yang and T.-C. Ou, *Appl. Catal. A*, 2006, **302**, 157-167.
45 C. Zhou, J. Yu, Y. Qin and J. Zheng, *Nanoscale*, 2012, **4**, 4228-4233.

Dalton Transactions Accepted Manuscript

 This journal is © The Royal Society of Chemistry 2013

46 V. Bondarenka, S. Grebinskij, S. Kaciulis, G. Mattogno, S. Mickevicius, H. Tvardauskas, V. Volkov and G. Zakharova, *J. Electron. Spectrosc. Relat. Phenom.*, 2001, **120**, 131-135.
47 Y. Zhang and R.J. Puddephatt, *Chem. Mater.*, 1999, **11**, 148-153.
48 W. Yao, X. Zheng, Y. Guo, W. Zhan, Y. Guo and G. Lu, *J. Mol. Catal. A*, 2011, **342-343**, 30-34.
49 X. Zhang, H. Yang and A. Tang, *J. Phys. Chem. B*, 2008, **112**, 16271-16297.
50 W.O. Gordon, B.M. Tissue and J.R. Morris, *J. Phys. Chem. C*, 2007, **111**, 3233-3240.
51 W. Yao, Y. Guo, X. Liu, Y. Guo, Y. Wang, Y. Wang, Z. Zhang and G. Lu, *Catal. Lett.*, 2007, **119**, 185-190.
52 H.-X. Zhong, Y.-L. Ma, X.-F. Cao, X.-T. Chen and Z.-L. Xue, *J. Phys. Chem. C*, 2009, **113**, 3461-3466.
53 X. Bai, H. Song, L. Yu, L. Yang, Z. Liu, G. Pan, S. Lu, X. Ren, Y. Lei and L. Fan, *J. Phys. Chem. B*, 2005, **109**, 15236-15242.
54 H. Wang, M. Yu, C. Lin, X. Liu and J. Lin, *J. Phys. Chem. C*, 2007, **111**, 11223-111230.
55 N. Zhang, X. Liu, R. Yi, R. Shi, G. Gao and G. Qiu, *J. Phys. Chem. C*, 2008, **112**, 17788-17795.
56 J.A. Nelson, E.L. Brant and M.J. Wagner, *Chem. Mater.*, 2003, **15**, 688-693.
57 X. Li, Q. Li, Z. Xia, L. Wang, W. Yan, J. Wang and R.I. Boughton, *Cryst. Growth Des.*, 2006, **6**, 2193-2196.
58 A.K. Parchur and R.S. Ningthoujam, *RSC Adv.*, 2012, **2**, 10859-10868.
59 C. Strohhöfer and A. Polman, *Appl. Phys. Lett.*, 2002, **81**, 1414-1416.
60 H. Zhu, X. Chen, Z. Zheng, X. Ke, E. Jaatinen, J. Zhao, C. Guo, T. Xie and D. Wang, *Chem. Comm.*, 2009, 7524-7526.
61 K. Toshikiyo, M. Tokunaga, S. Takeoka, M. Fujii and S. Hayashi, *J. Appl. Phys.*, 2001, **89**, 4917-4920.

Dalton Transactions Accepted Manuscript